analytical chemistry

pubs.acs.org/ac

Technical Note

Integration of Trapped Ion Mobility Spectrometry and Ultraviolet Photodissociation in a Quadrupolar Ion Trap Mass Spectrometer

Miguel Santos-Fernandez, Kevin Jeanne Dit Fouque, and Francisco Fernandez-Lima*

Cite This: *Anal. Chem.* 2023, 95, 8417−8422

Read Online

ACCESS | Metrics & More | Article Recommendations | Supporting Information

ABSTRACT: There is a growing demand for lower-cost, benchtop analytical instruments with complementary separation capabilities for the screening and characterization of biological samples. In this study, we report on the custom integration of trapped ion mobility spectrometry and ultraviolet photodissociation capabilities in a commercial Paul quadrupolar ion trap multistage mass spectrometer (TIMS-QIT-MS^n UVPD platform). A gated TIMS operation allowed for the accumulation of ion mobility separated ion in the QIT, followed by a mass analysis (MS1 scan) or m/z isolation, followed by selected collision induced dissociation (CID) or ultraviolet photodissociation (UVPD) and a mass analysis (MS2 scan). The analytical potential of this platform for the analysis of complex and labile biological samples is illustrated for the case of positional isomers with varying PTM location of the histone H4 tryptic peptide 4-17 singly and doubly acetylated and the histone H3.1 tail (1-50) singly trimethylated. For all cases, a baseline ion mobility precursor molecular ion preseparation was obtained. The tandem CID and UVPD MS2 allowed for effective sequence confirmation as well as the identification of reporter fragment ions associated with the PTM location; a higher sequence coverage was obtained using UVPD when compared to CID. Different from previous IMS-MS implementation, the novel TIMS-QIT-MS^n UVPD platform offers a lower-cost alternative for the structural characterization of biological molecules that can be widely disseminated in clinical laboratories.

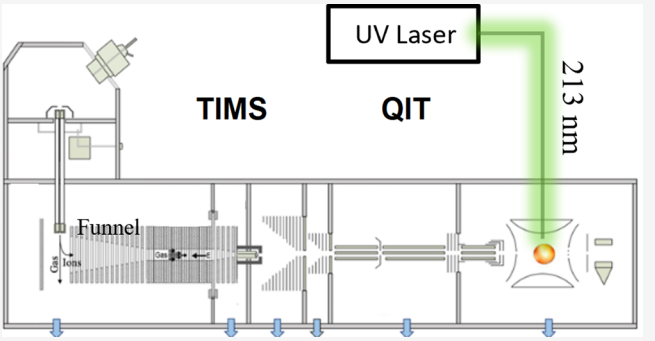

Downloaded via FLORIDA INTL UNIV on June 11, 2024 at 16:09:51 (UTC).
See https://pubs.acs.org/sharingguidelines for options on how to legitimately share published articles.

INTRODUCTION

In recent years, ion mobility spectrometry (IMS) have been increasingly used for a wide diversity of applications, varying from small molecule detection to large macromolecular complex structural characterization.[1−3] In a traditional drift tube IMS (DTIMS) device, ions are separated in the gas-phase based on their differences in ion mobility as they drift through a region filled with a buffer gas under an external electric field.[4] Different from traditional IMS devices, trapped IMS (TIMS) separation is based on holding the ions stationary using an electric field against a moving buffer gas, followed by their sequential release.[5] An *rf* is applied to the TIMS electrodes, generating a radially confining pseudopotential, while an axial electric field gradient is produced across the electrodes to counteract the drag force exerted by the gas flow, effectively leading to the trapping of the ions.[6] The analytes are subsequently eluted from the analyzer as the magnitude of the axial electric field is progressively decreased. Since the introduction of TIMS in 2011,[5] multiple studies have shown the potential of this technique for a wide range of bioanalytical applications, including small molecules,[7] petroleomic,[8] lipidomic,[9] catalysis,[10] coenzymes,[11] peptides,[12] proteins,[13] polymers,[14] DNA,[15] glycomic,[16] and proteomics.[17] The commercialization in 2015 of the timsTOF series by Bruker Daltonics Inc. enabled access to the scientific community at large to this technology.

Over the years, several groups have successfully coupled IMS devices to a variety of mass spectrometers, including time-of-flight (ToF),[18] linear ion trap,[19] quadrupole ion trap,[20] orbitrap,[21] and Fourier transform ion cyclotron resonance (FT-ICR).[22] In addition to the commercial timsTOF series by Bruker Daltonics Inc., three more commercial alternatives are available, consisting of the Agilent DTIMS-q-ToF MS, the Waters q-(c)TWIMS-ToF MS, and the Thermo FAIMS-q-Orbitrap MS platforms A common characteristic is that all three platforms can be easily integrated with LC workflows and allow for tandem MS/MS using collision-induced dissociation (CID). While these instruments have found multiple applications, they are still high-end ticket MS platforms.

Received: March 20, 2023
Accepted: May 9, 2023
Published: May 23, 2023

ACS Publications

© 2023 American Chemical Society

In this technical note, we report for the first time on the custom integration of TIMS and ultraviolet photodissociation (UVPD) capabilities in a commercial Paul quadrupolar ion trap multistage mass spectrometer (TIMS-QIT-MS^n UVPD). This lower-cost, benchtop analytical instrument offers complementary separation capabilities for the screening and characterization of biological samples and can be easily integrated in clinical laboratories. The analytical potential of this platform is illustrated for the case of positional isomers with varying PTM location of the histone H4 tryptic peptide 4-17 singly and doubly acetylated and the histone H3.1 tail (1-50) singly trimethylated. The added UVPD has unique advantages for the structural characterization of biological samples.[23] UVPD fragmentation relies on the absorption of UV photons, which excite ions electronically, leading to direct dissociation from the exited states via high-energy dissociation pathways (a_i/x_i series ions unique to UVPD) and/or through relaxation processes involving lower-energy fragmentation pathways (b_i, c_i/y_i, z_i series ions).[24,25] UVPD's ability to generate a vast range of product ions with higher fragmentation efficiency, when compared to electron-capture dissociation (ECD), significantly improves the sequence coverage and boosts the level of confidence in peptide and protein characterization. Additionally, UVPD can conserve and pinpoint post-translational modifications (PTMs)[26] and ligand binding sites,[27] as well as break disulfide/thioether bonds.[28]

EXPERIMENTAL SECTION

Peptide and Sample Preparation. Synthesized tryptic digested histone H4 (4-17) singly (K5Ac and K8Ac, 1312 Da) and doubly acetylated (K5AcK8Ac and K8AcK16Ac, 1354 Da) peptides, as well as histone tail H3.1 (1-50) singly trimethylated (TriMetK4 and TriMetK27, 5380 Da) were obtained from GenScript (Piscataway, NJ). All peptide solutions were analyzed at a concentration of 15 μM prepared in 50:50 water/methanol (H_2O/MeOH) with 0.1% formic acid. A low-concentration Tuning Mix standard (G1969-85000) was obtained from Agilent Technologies (Santa Clara, CA) and used for external ion mobility and mass calibration purposes.

TIMS-QIT-MSn UVPD Platform. The TIMS and UVPD capabilities were integrated on a commercial Bruker Amazon Speed quadrupole ion trap mass spectrometer (Bruker Daltonics Inc., Billerica, MA). Figure 1A shows a simplified schematic of the nESI- TIMS-QIT-MSn UVPD. The general fundamentals of TIMS and calibration procedures have been previously reported in the literature.[5,6,29] The instrument was equipped with a custom-built nESI source operated in the positive ion mode. The nESI emitters were pulled in-house from quartz capillaries (O.D. = 1.0 mm and I.D. = 0.70 mm) using a Sutter Instrument Co. P2000 laser puller. Peptide sample solutions were loaded in a pulled-tip capillary, housed in a mounted custom-built XYZ stage in front of the MS inlet, and sprayed at ~900−1200 V via a tungsten wire inserted inside the nESI emitters.

TIMS experiments were performed using nitrogen (N_2) at ambient temperature (T) and a few Torr. The TIMS unit was controlled by a modular intelligent power source (MIPS, GAA Custom Electronics, WA), consisting of 16 channels with a ±250 V output range and two rf drivers. TIMS was operated using an rf amplitude and frequency of 320 Vpp and 1040 kHz, and the multipole using an rf voltage and frequency of 174 Vpp at 904 kHz. A deflector voltage of 250 V, a TIMS exit lens of

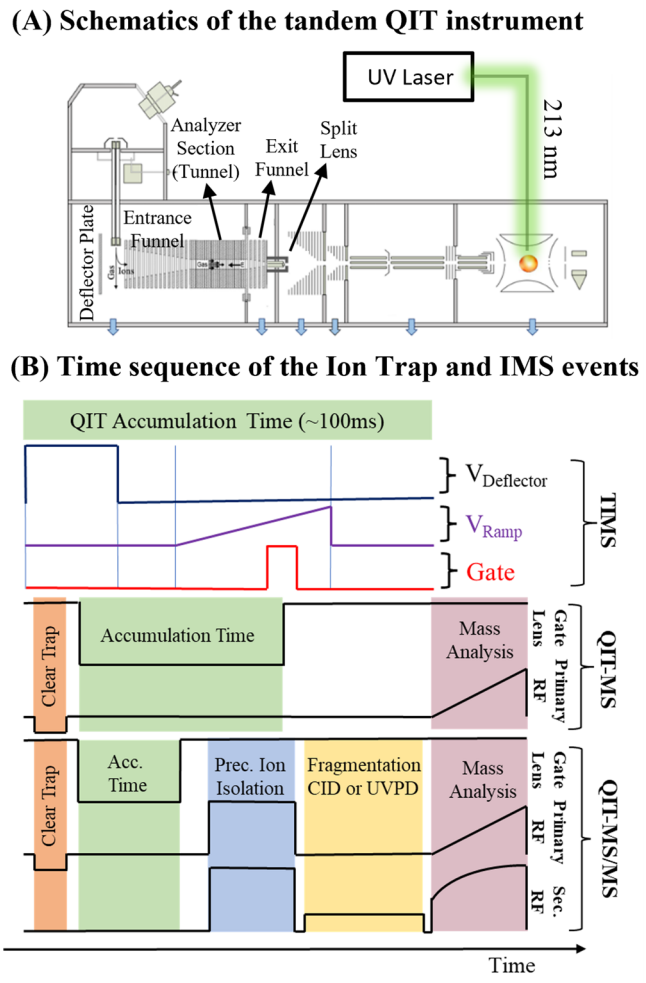

Figure 1. (A) Schematic of the tandem TIMS-QIT-MS^n UVPD instrument. (B) Time sequence of the ion trap and IMS events.

145 V, a multipole exit lens (gate) of 140 V, as well as a ramp voltage of −86 to −80 V (singly acetylated H4 peptide), −67 to −53 V (doubly acetylated H4 peptide), and −140 to −120 V (H3.1 tails) were used for the ion mobility separations. The scan rate (Sr = $\Delta V_{ramp}/t_{ramp}$) was optimized for high ion mobility separation.

The timing sequence for the TIMS-QIT-MS and TIMS-QIT-MS/MS are described in Figure 1B. The QIT accumulation time event was used to trigger the MIPS, which then controlled the IMS events and the UVPD events. The TIMS radial confinement was optimized by changing the rf amplitude (Figure S1). Briefly, ions are orthogonally deflected into the TIMS device (open for 9 ms using a Δ150 V at the deflector), trapped and eluted using a nonlinear ramp scan such that higher mobility resolution is achieved over the ion mobility range of interest.[30] The analytical section of the nonlinear ramp consisted of a ΔV ramp of 6 V (singly acetylated H4 peptide), 14 V (doubly acetylated H4 peptide), and 20 V (H3.1 tails). The ion mobility range of interest that is transferred into the QIT is defined by the ion gate located in the split lens (Figure S2); a typical gate pulse of 2 ms width, 0.1 ms steps, and a ΔV_{Gate} = 100 V were used. The MIPS generated a delayed pulse to control the UVPD shutter. A 213 nm laser beam, generated from the fifth harmonic of a Nd:YAG laser (NL204, EKSPLA, Vilnius, Lithuania), was

https://doi.org/10.1021/acs.analchem.3c01220
Anal. Chem. 2023, 95, 8417−8422

operated at a repetition rate of 1 kHz with an energy of ∼0.2 mJ per pulse with a 8 ns pulse width. The optical path consisted of UV-enhanced aluminum mirrors used to guide the beam, UV fused silica flange-mounted windows (vacuum−atmosphere interface), and an optical shutter (SH-20, Electro-Optical Products Corp., Ridgewood, NY). The MS/MS spectra were annotated manually using a $S/N > 6$. All resolving power (R) and resolution (r) values reported herein were determined as $R = \Omega/w$ and $r = 1.18(\Omega 2 - \Omega 1)/(w1 + w2)$, where Ω and w are collision cross sections (CCS) and the full peak width at half-maximum (fwhm) of the IMS profile.

RESULTS AND DISCUSSION

TIMS-QIT MS/MS of Isomeric H4 4-17 K8Ac and K5Ac. The nESI-MS analysis of the H4 (4-17) K5Ac and K8Ac positional isomers in denaturing solution conditions showed a charge state distribution, ranging from $[M + H]^+$ to $[M + 3H]^{3+}$ molecular species, with the $[M + 3H]^{3+}$ ions (m/z 439) being the most predominant (Figure S3). The TIMS-QIT-MS and TIMS-QIT-MS/MS experiments were performed on the $[M + 3H]^{3+}$ (m/z 439) charge state using a 1:1 v-v mixture. A near baseline ion mobility separation ($R \approx 136$ and a $r \approx 1.2$) of the two positional isomers was observed using Sr = 0.38 V/ms (Figure 2A). The confirmation for each ion mobility band was obtained from the reported fragment ions y_{12}^{2+} at m/z 543 for K5Ac (purple lines) and m/z 564 for K8Ac (green lines) as a function of the collision energy.

Additional confirmations were obtained from the IMS-MS and IMS-MS/MS analysis of each single peptide (Figures S3 and S4). The unique fragmentation patterns yielded the PTM location, as well as the sequence confirmation, with a sequence coverage of 65% for both peptides (Figure 2B). CID fragmentation of K5Ac showed the presence of the b_2^+ fragment ions (m/z 227) with a 42 Da shift, corresponding to an acetylation, confirming the position of the PTM at K5. In the case of K8Ac the CID fragmentation yielded the presence of b_3^+ and y_7^+ (m/z 285 and 673 respectively) both without any shift, as well as the presence of y_{12}^{2+} (m/z 564) with a 42 Da shift, corroborating the position of the PTM at the K8 position. This implies that the present acetylation PTMs are not labile and can be detected using CID techniques.

In addition, UVPD fragmentation showed common a_i, b_i, c_i/x_j, y_j, and z_j product ions for the two positional isomers and a fragmentation efficiency of ∼20% (Figure S5A,B). Reporter fragment ions y_{12}^{2+} were also present in the UVPD fragmentation spectra, as well as fragment ions b_2 (m/z 227) with a 42 Da shift corresponding to an acetylation in the K5 position for the case of K5Ac, and fragment ions a_4^+ (m/z 314) and c_6^{2+} (m/z 470) with a mass shift of 42 Da (Figure S5A,B), which permitted the assignment of the PTM locations. When compared with CID, UVPD showed full sequence coverage, indicating higher confidence level in assigning PTM locations.

TIMS-QIT MS/MS of Isomeric H4 4-17 K5AcK8Ac and K8AcK16Ac. The nESI-MS analysis of the H4 (4-17) K5AcK8Ac and K8AcK16Ac positional isomers in denaturing solution conditions showed a charge state distribution, ranging from $[M + H]^+$ to $[M + 3H]^{3+}$ molecular species, with the $[M + 3H]^{3+}$ ions (m/z 452) being the most predominant (Figures S6). The TIMS-QIT-MS and TIMS-QIT-MS/MS experiments were performed on the $[M + 3H]^{3+}$ (m/z 452) charge state using a 1:1 v-v mixture. A baseline ion mobility separation ($R \approx 70$ and a $r \approx 1.2$) of the two positional isomers was observed using Sr = 0.35 V/ms (Figure 3A). The confirmation of each

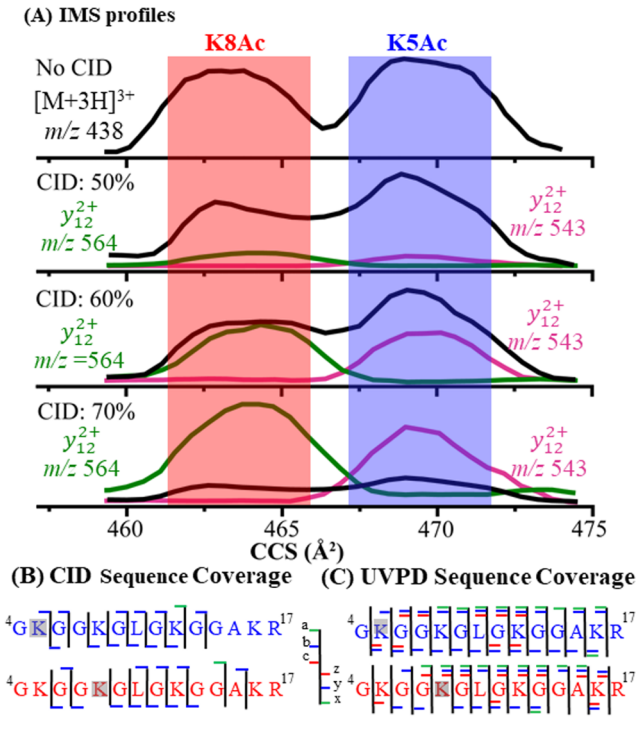

Figure 2. (A) Ion mobility profiles of the $[M + 3H]^{3+}$ species from K5Ac (red rectangle) and K8Ac (blue rectangle) binary mixture (black line), and of reporter ions y_{12}^{2+} (m/z 543 purple lines for K5Ac, and m/z 564 green lines for K8Ac) as a function of the collision energy. (B and C) CID and UVPD sequence coverage of K5Ac (blue) and K8Ac (red), respectively.

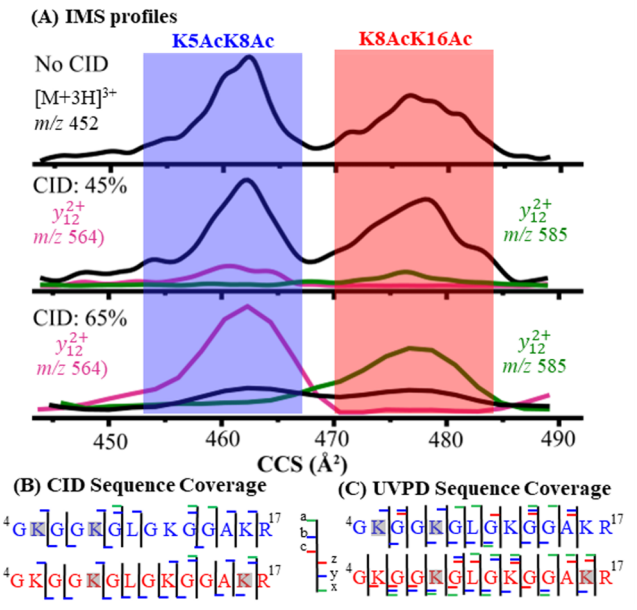

Figure 3. (A) Ion mobility profiles of the $[M + 3H]^{3+}$ species from K5AcK8Ac (blue rectangle) and K8AcK16Ac (red rectangle) binary mixture (black lines), and reporter ions y_{12}^{2+} (m/z 564, purple lines for K5AcK8Ac and m/z 585, green lines for K8AcK16Ac) as a function of the collision energy. (B and C) CID and UVPD sequence coverage of K5AcK8Ac (blue) and K8AcK16Ac (red), respectively.

https://doi.org/10.1021/acs.analchem.3c01220
Anal. Chem. 2023, 95, 8417−8422

ion mobility band was obtained from the reported fragment ions y_{12}^{2+} at m/z 564 (purple lines) for K5AcK8Ac and m/z 585 (green lines) for K8AcK16Ac as a function of the collision energy.

Additional confirmation was obtained from the IMS-MS and IMS-MS/MS analysis for each single peptide (Figures S6 and S7). The CID unique fragmentation patterns resulted in the PTM location, as well as the sequence confirmation, with a sequence coverage of 65% for K5AcK8Ac and 79% for K8AcK16Ac. Reporter ions b_2^+ (m/z 228) with a 42 Da shift corresponding to an acetylation in the position K5, as well as b_5^+ (m/z 512) with a 42 Da shift together with y_9^{2+} (m/z 422) without any shift confirmed the acetylation positions for K5AcK8Ac (Figures S6 and 7A). The CID spectrum for K8AcK16Ac (Figures S6 and 7B) yielded the presence of y_2^+ and y_6^+ (m/z 345 and 658, respectively) fragment ions with a 42 Da shift, as well as the appearance of fragment ions y_{12}^{2+} (m/z 685) with an 84 Da shift confirming the PTM positions. Common a_i, b_i, c_i/x_j, y_j, and z_j product ions were observed in the UVPD fragmentation spectra of the molecular ions $[M + 3H]^{3+}$ (m/z 452) with 40% UVPD fragmentation efficiency (Figure S8). Fragment ions c_3^+ (m/z 302) with a 42 Da shift corresponding to the acetylation and b_5^+ (m/z 302) with an 84 Da mass shift corresponding to two acetylations mass shift corresponding to two acetylations corroborate the positions of both PTMs in K5 and K8, respectively. For the case of K8AcK16Ac fragment ions y_2^+ (m/z 345) and y_6^+ (m/z 658) with a 42 Da mass shift corresponding to an acetylation in the K16 position was observed, as well as fragment ion x_{10}^{2+} (m/z 541) with a 84 Da mass shift corresponding to two acetylations, one in position K16 and the other one in position K8. When compared with CID, UVPD showed 85% sequence coverage, increasing the confidence level in assigning PTM locations.

TIMS-QIT MS/MS of Isomeric H3.1 TriMetK4 and TriMetK27 Tails. The nESI-MS analysis of the H3.1 (1-50) TriMetK4 and TriMetK27 positional isomers in denaturing solution conditions showed a charge state distribution, ranging from $[M + 8H]^{8+}$ to $[M + 12H]^{12+}$ molecular species, with the $[M + 10H]^{10+}$ ions (m/z 539) being the most predominant (Figure S9). The TIMS-QIT-MS and TIMS-QIT-MS/MS experiments were performed on the $[M + 10H]^{10+}$ (m/z 539) molecular ion using a 1:1 v-v mixture. A baseline ion mobility separation ($R \approx 160$ and a $r \approx 1.0$) of the two positional isomers was observed using a Sr = 0.5 V/ms (Figure 4A). Complementary validation of the ion mobility profiles was achieved by varying the starting peptide molar ratios: 1:2, 1:1, and 2:1 (Figure S10) using the same experimental settings. For the case of the 1:2 TriMetK4:TriMetK27 molar ratio, an appreciable increase on the intensity of the ion mobility band at 1818 A^2, corresponding to the TriMetK27, was observed; analogously, for the 2:1 TriMetK4:TriMetK27 molar ratio, there was also a change in the ion mobility band at 1840 A^2 corresponding to the TriMetK4.

TIMS CID MS/MS analysis of the $[M + 10H]^{10+}$ molecular ions yielded a sequence coverage of ~46% and ~82% for TriMetK27 and TriMetK4, respectively, as well as the location of the PTMs (Figure 4B). The comparison of the ion mobility selected CID MS/MS spectra showed unique reporter fragment ions for each positional isomer. For example, in the m/z 300−500 range the presence of the b_9^{3+} reporter ion with and without the 42 Da shift corresponding to a trimethylation clearly separated the two isomers (Figure S11). The presence

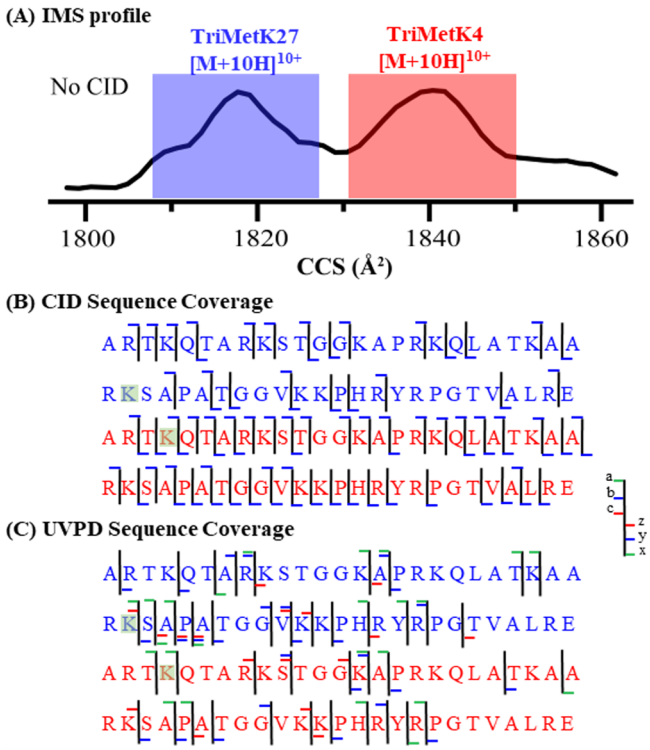

Figure 4. (A) Ion mobility profiles of the $[M + 10H]^{10+}$ species from TriMetK27 (blue rectangle) and TriMetK4 (red rectangle) binary mixture (black lines). (B and C) CID and UVPD sequence coverage of TriMetK27 (blue) and TriMetK4 (red), respectively.

of the b_8^{3+} product ions (m/z 319) with a 42 Da shift on the MS/MS spectra corroborated the PTM location for the TriMetK4 peptide. In the case of TriMetK27, the presence of the fragment ions y_{26}^{4+} with a shift of 42 Da (m/z 712), as well as the presence of the fragment ions b_{25}^{4+} and y_{17}^{3+} (m/z 652 and 656 respectively) without any shift, confirmed the position of the trimethylation for TriMetK27.

The UVPD MS/MS analysis of the $[M + 10H]^{10+}$ molecular ions of the positional isomers showed common a_i, b_i, c_i/x_j, y_j, and z_j product ions with a UVPD fragmentation efficiency of 34% (Figure S12). The presence of reporter ion a_{23}^{4+} (m/z 610) without any mass shift, as well as reporter ion c_{27}^{6+} (m/z 493) with a 42 Da shift, yielded the position of the PTM for TriMetK27. In the case of TriMetK4, the presence of a_4^{2+} (m/z 236) and a_{42}^{9+} (m/z 502), both with a 42 Da mass shift, corroborates the position of the PTM. When compared to CID, UVPD provided a sequence coverage of ~45%. The presence of a lower sequence coverage using UVPD, as compared to CID, probably arises from the mass resolution limitation of the ion trap analyzer together with lower fragmentation efficiency (lower signal intensity), which makes the fragment ion assignments more challenging especially for highly charged product ions, for which the isotopic distribution patterns will not be resolved. In fact, we recently showed that the use of UVPD fragmentation in a ToF MS platform resulted in a sequence coverage of ~84% for TriMetK27 and TriMetK4.[26]

CONCLUSIONS

The analysis of three isomeric/isobaric mixtures allowed the performance evaluation of the novel TIMS-QIT-MS^n strategy.

https://doi.org/10.1021/acs.analchem.3c01220
Anal. Chem. 2023, 95, 8417−8422

The TIMS high mobility resolving power was achieved in all examples shown. The advantages of ion mobility preseparation were demonstrated effectively with positional isomers/isobars of peptides with varying PTM positions; the examples shown are traditional challenges encountered during the analysis of histone samples. The peptide sequence and PTM positions were derived from ion mobility-separated MS/MS scans using both CID and UVPD fragmentation mechanisms; however, UVPD showed to be more efficient with a better sequence coverage, increasing the level of confidence in assigning PTMs.

Different from previous TIMS-MS implementation, the QIT lower cost and MS/MS capabilities significantly enhance the possibility for wider implementation of complementary ion mobility and mass analysis in lower-budget clinical/service laboratories and educational/academic environments. The TIMS-QIT MS/MS showed great applicability for the analysis of low charge state peptides (z = +1 to +3) typically obtained in bottom-up proteomic applications. Moreover, the lower QIT mass resolution and m/z range when compared to ToF and FT-ICR MS instruments can limit their applicability to middle- and top-down proteomics applications (e.g., over 50 amino acids with z > 5+).

■ ASSOCIATED CONTENT

Supporting Information

The Supporting Information is available free of charge at https://pubs.acs.org/doi/10.1021/acs.analchem.3c01220.

Figures illustrating the effects of *rf* drive, TIMS gate steps width, experiment time and cycles on the peak shape and peak separation for tuning mix; MS, CID MS/MS, and UVPD MS/MS spectra for K5Ac, K8Ac, K5AcK8Ac, K8AcK16Ac, TriMetK4, TriMetK27, and their mixtures; individual mobility profiles for K5Ac, K8Ac, K5AcK8Ac, and K8AcK18Ac with and without CID; mobility spectra with different molar ratios of TriMetK4 and TriMetK27; zoomed in area of mobility-selected CID spectra for TriMetK4 and TriMetK27 (PDF)

■ AUTHOR INFORMATION

Corresponding Author

Francisco Fernandez-Lima − *Department of Chemistry and Biochemistry and Biomolecular Science Institute, Florida International University, Miami, Florida 33199, United States;* orcid.org/0000-0002-1283-4390; Email: fernandf@fiu.edu

Authors

Miguel Santos-Fernandez − *Department of Chemistry and Biochemistry, Florida International University, Miami, Florida 33199, United States;* orcid.org/0000-0003-4233-0203

Kevin Jeanne Dit Fouque − *Department of Chemistry and Biochemistry, Florida International University, Miami, Florida 33199, United States*

Complete contact information is available at: https://pubs.acs.org/10.1021/acs.analchem.3c01220

Author Contributions

The manuscript was written through contributions of all authors. All authors approved the final version of the manuscript.

Notes

The authors declare no competing financial interest.

■ ACKNOWLEDGMENTS

The authors acknowledge the financial support from National Institutes of General Medicine (R01GM134247) to F.F.-L. We thank Dr. Mark E. Ridgeway (Bruker Daltonics Inc.), Dr. Christoph Gebhardt (Bruker Daltonics GmbH), and Eng. Gordon Anderson (GAA Custom Electronics, LLC) for helpful discussions and technical support. M.S.-F. acknowledges the support from National Science Foundation (HRD-1547798 and No. HRD-2111661) as a fellow of the Centers of Research Excellence in Science and Technology (CREST) Program.

■ REFERENCES

(1) Borsdorf, H.; Eiceman, G. A. *Appl. Spectrosc. Rev.* **2006**, *41* (4), 323−375.
(2) Lapthorn, C.; Pullen, F.; Chowdhry, B. Z. *Mass. Spectrom. Rev.* **2013**, *32* (1), 43−71.
(3) Jeanne Dit Fouque, K.; Fernandez-Lima, F. *Trends Anal. Chem.* **2019**, *116*, 308−315.
(4) Zeleny, J. *London Edinb. Dublin Philos. Mag. J. Sci.* **1898**, *46* (278), 120−154.
(5) Fernandez-Lima, F.; Kaplan, D. A.; Suetering, J.; Park, M. A. *Int. J. Ion Mobil. Spectrom.* **2011**, *14* (2-3), 93.
(6) Hernandez, D. R.; Debord, J. D.; Ridgeway, M. E.; Kaplan, D. A.; Park, M. A.; Fernandez-Lima, F. *Analyst.* **2014**, *139* (8), 1913−1921.
(7) Adams, K. J.; Ramirez, C. E.; Smith, N. F.; Munoz-Munoz, A. C.; Andrade, L.; Fernandez-Lima, F. *Talanta* **2018**, *183*, 177−183.
(8) Benigni, P.; Sandoval, K.; Thompson, C. J.; Ridgeway, M. E.; Park, M. A.; Gardinali, P.; Fernandez-Lima, F. *Environ. Sci. Technol.* **2017**, *51* (11), 5978−5988.
(9) Jeanne Dit Fouque, K.; Ramirez, C. E.; Lewis, R. L.; Koelmel, J. P.; Garrett, T. J.; Yost, R. A.; Fernandez-Lima, F. *Anal. Chem.* **2019**, *91* (8), 5021−5027.
(10) Greisch, J.-F.; Weis, P.; Brendle, K.; Kappes, M. M.; Haler, J. R. N.; Far, J.; De Pauw, E.; Albers, C.; Bay, S.; Wurm, T.; Rudolph, M.; Schulmeister, J.; Hashmi, A. S. K. *Organometallics* **2018**, *37* (9), 1493−1500.
(11) Molano-Arevalo, J. C.; Hernandez, D. R.; Gonzalez, W. G.; Miksovska, J.; Ridgeway, M. E.; Park, M. A.; Fernandez-Lima, F. *Anal. Chem.* **2014**, *86* (20), 10223−10230.
(12) Jeanne Dit Fouque, K.; Hegemann, J. D.; Santos-Fernandez, M.; Le, T. T.; Gomez-Hernandez, M.; van der Donk, W. A.; Fernandez-Lima, F. *Anal. Bioanal. Chem.* **2021**, *413*, 4815.
(13) Ridgeway, M. E.; Silveira, J. A.; Meier, J. E.; Park, M. A. *Analyst.* **2015**, *140* (20), 6964−6972.
(14) Haler, J. R. N.; Massonnet, P.; Chirot, F.; Kune, C.; Comby-Zerbino, C.; Jordens, J.; Honing, M.; Mengerink, Y.; Far, J.; Dugourd, P.; De Pauw, E. *J. Am. Soc. Mass Spectrom.* **2018**, *29* (1), 114−120.
(15) Butcher, D.; Chapagain, P.; Leng, F.; Fernandez-Lima, F. *J. Phys. Chem. B* **2018**, *122* (27), 6855−6861.
(16) Pu, Y.; Ridgeway, M. E.; Glaskin, R. S.; Park, M. A.; Costello, C. E.; Lin, C. *Anal. Chem.* **2016**, *88* (7), 3440−3443.
(17) Meier, F.; Beck, S.; Grassl, N.; Lubeck, M.; Park, M. A.; Raether, O.; Mann, M. *J. Proteome. Res.* **2015**, *14* (12), 5378−5387.
(18) Fernandez-Lima, F. A.; Kaplan, D. A.; Park, M. A. *Rev. Sci. Instrum.* **2011**, *82* (12), 126106.
(19) Zucker, S. M.; Lee, S.; Webber, N.; Valentine, S. J.; Reilly, J. P.; Clemmer, D. E. *J. Am. Soc. Mass Spectrom.* **2011**, *22* (9), 1477−1485.
(20) Hoaglund, C. S.; Valentine, S. J.; Clemmer, D. E. *Anal. Chem.* **1997**, *69* (20), 4156−4161.
(21) Poltash, M. L.; McCabe, J. W.; Shirzadeh, M.; Laganowsky, A.; Clowers, B. H.; Russell, D. H. *Anal. Chem.* **2018**, *90* (17), 10472−10478.

(22) Ridgeway, M. E.; Wolff, J. J.; Silveira, J. A.; Lin, C.; Costello, C. E.; Park, M. A. *Int. J. Ion Mobil. Spectrom.* **2016**, *19* (2), 77−85.
(23) Shaw, J. B.; Li, W.; Holden, D. D.; Zhang, Y.; Griep-Raming, J.; Fellers, R. T.; Early, B. P.; Thomas, P. M.; Kelleher, N. L.; Brodbelt, J. S. *J. Am. Chem. Soc.* **2013**, *135* (34), 12646−12651.
(24) Antoine, R.; Dugourd, P. *Phys. Chem. Chem. Phys.* **2011**, *13* (37), 16494−16509.
(25) R. Julian, R. *J. Am. Soc. Mass. Spectrom.* **2017**, *28* (9), 1823−1826.
(26) Miller, S. A.; Jeanne Dit Fouque, K.; Ridgeway, M. E.; Park, M. A.; Fernandez-Lima, F. *J. Am. Soc. Mass. Spectrom.* **2022**, *33* (7), 1267−1275.
(27) Sipe, S. N.; Patrick, J. W.; Laganowsky, A.; Brodbelt, J. S. *Anal. Chem.* **2020**, *92* (1), 899−907.
(28) Bonner, J.; Talbert, L. E.; Akkawi, N.; Julian, R. R. *Analyst.* **2018**, *143* (21), 5176−5184.
(29) Ridgeway, M. E.; Lubeck, M.; Jordens, J.; Mann, M.; Park, M. A. *Int. J. Mass Spectrom.* **2018**, *425*, 22−35.
(30) Benigni, P.; Porter, J.; Ridgeway, M. E.; Park, M. A.; Fernandez-Lima, F. *Anal. Chem.* **2018**, *90* (4), 2446−2450.

https://doi.org/10.1021/acs.analchem.3c01220
Anal. Chem. 2023, 95, 8417−8422